Quenching and Vibrational Relaxation of SO($B^3\Sigma^-$, $v' \leq 3$) by Collisions with Ar and N_2

Takayuki Hatano,[†] Shinji Watanabe,[†] Hidekazu Fujii,[†] Ikuo Tokue,[†] and Katsuyoshi Yamasaki*[,‡]

Department of Chemistry, Niigata University, Ikarashi, Niigata 950-2181, Japan and Department of Chemistry, Graduate School of Science, Hiroshima University, 1-3-1 Kagamiyama, Higashi-Hiroshima, Hiroshima 739-8526, Japan

Received: October 21, 2006; In Final Form: December 14, 2006

Fluorescence from a single vibronic level of SO($B^3\Sigma^-$, $v' \leq 3$) prepared by a pulse excitation has been detected and thorough kinetic analyses for the photochemical processes have been made. Deconvolution analysis by the integrated-profiles method of the time-resolved fluorescence profiles recorded at various buffer gas (Ar and N_2) pressures has given the deactivation rates of initially prepared vibrational levels. Componential analysis of the dispersed fluorescence measured at different buffer gas pressures has provided the rate coefficients for level-to-level vibrational relaxation. It has been found that not only the single-quantum relaxation ($\Delta v = 1$) but also the multiquantum relaxation ($\Delta v = 2$ and 3) occurs by collisions with Ar and N_2. The efficiency of quenching is strongly dependent on the vibrational levels and correlates with the energies of the lowest nonfluorescent rotational levels. Candidates for the electronic states governing the quenching process have been discussed based on the kinetic and spectroscopic data.

Introduction

The dipole transitions between two electronic states with largely different internuclear distances are appropriate for making widely tunable lasers. For example, SO has been a target as a medium of optically, chemically, or discharge pumped tunable ultraviolet laser.[1−7] The lasing in the $B^3\Sigma^- - X^3\Sigma^-$ system (Figure 1) with many closely spaced rovibrational dipole-allowed transitions offers a line-tunable ultraviolet source.

The ultraviolet lasing by optically pumped SO has first been reported by Miller et al.[6] They have generated SO in the photolysis of SO_2 at 193 nm and demonstrated stimulated emission in the $v' = 0 \rightarrow v'' = 8-11$ bands of the $B^3\Sigma^-$-$X^3\Sigma^-$ system. Stuart et al.[7] have also photolyzed SO_2 at 193 nm and found six new bands of lasing from vibrationally excited levels in the $B^3\Sigma^-$ state: $v' = 1 \rightarrow v'' = 6$ and 7 and $v' = 2 \rightarrow v'' =$ 4, 5, 6, and 10. They have measured the effects of rotational mixing (relaxation) and saturation fluence by collisions with buffer gases (He and Ar), finding that quenching and/or vibrational relaxation lower the efficiency of lasing. Their data are useful to improve the gain of the SO lasing; however, the results are limited to the phenomenological properties. More basic kinetic measurements of quenching and vibrational relaxation are necessary for characterizing the lasing action of SO($B^3\Sigma^-$).

The rotational levels of $v' = 0-3$, $66 \leq N'$ ($v' = 0$), $54 \leq N'$ ($v' = 1$), $38 \leq N'$ ($v' = 2$), and $11 \leq N'$ ($v' = 3$), and all of $v' > 3$ of the $B^3\Sigma^-$ state of $^{32}S^{16}O$ are nonfluorescent.[8] The cause of nonradiative decay has been thought to be predissociation via a repulsive or weakly bound $^3\Pi$ state[8,9] for almost 70 years since Martin[9] found the cutoff in the rotationally resolved emission spectra. Ornellas and Borin,[10,11] however, have recently performed the ab initio calculations, suggesting that the perturbing $^3\Pi$ state has a distinct well formed by avoided crossing with another $^3\Pi$ state and has eight vibrational levels. The energetically low and high adiabatic $^3\Pi$ states have designated $C^3\Pi$ and $C'^3\Pi$ states, respectively. Ornellas and Borin have also shown that the potential energy curve of the $C^3\Pi$ state crosses the $B^3\Sigma^-$ state at an internuclear distance of 0.164 nm and that the rotational levels corresponding to the energies at the intersection, $N' = 66$ ($v' = 0$), 54 ($v' = 1$), 40 ($v' = 2$), and 16 ($v' = 3$), are in good agreement with the lowest nonfluorescent levels reported by Clerbaux and Colin.[8] Furthermore, Archer et al.[12] have directly observed two vibrational levels ($v' = 0$

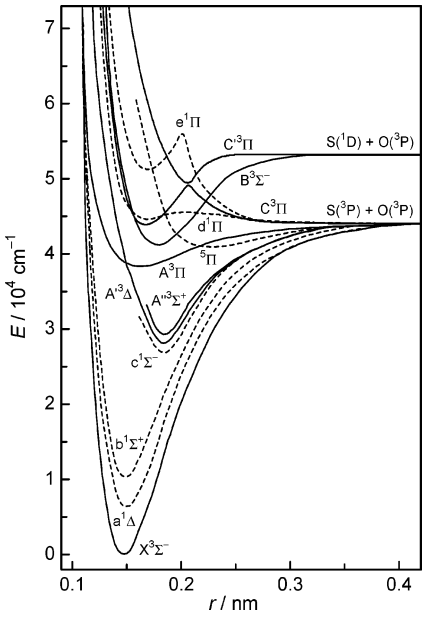

Figure 1. Potential energy curves for the electronic states of SO. The solid curves are triplet states and the dashed curves are singlet and quintet states.

* Corresponding author. E-mail: kyam@hiroshima-u.ac.jp. Fax: +81-82-424-7405.
[†] Niigata University.
[‡] Hiroshima University.

10.1021/jp066907m CCC: $37.00
Published on Web 01/27/2007

and 1) of the $C^3\Pi$ state by jet cooled 1 + 1 multiphoton ionization spectroscopy and reported that $v' = 0$ of $C^3\Pi$ is located between $v' = 4$ and 5 of the $B^3\Sigma^-$ state. They also have observed no fluorescence on exciting the vibrational levels of the $C^3\Pi$ state, suggesting a predissociation.

These findings have motivated us to clarify the mechanism governing the photochemical processes in the $B^3\Sigma^-$ state. We have reported the radiative lifetimes and deactivation rate coefficients of SO($B^3\Sigma^-$, $v' \leq 3$) by collisions with He.[13−15] The present study lays a target on the photochemistry of the fluorescent vibrational levels $v' \leq 3$ of the $B^3\Sigma^-$ state by collisions with Ar and N_2 based on the thorough kinetic analysis of time- and wavelength-resolved fluorescence from a single vibrational level.

Experimental Section

The experimental apparatus has been described previously.[13−15] SO_2 (3 mTorr) at 298 ± 2 K in a buffer gas (Ar or N_2, ≤ 200 Torr) was photolyzed at 193.3 nm with an ArF excimer laser (Lambda Physik LEXtra50, 19 Hz) and SO($X^3\Sigma^-$) was generated. The following two channels are energetically possible in the 193.3 nm photolysis [$h\nu$ (193.3 nm) = 619 kJ mol^{-1}].

$$SO_2 \rightarrow SO(X^3\Sigma^-) + O(^3P) \quad \Delta H° = 551 \text{ kJ mol}^{-1} \quad (1)$$

$$\rightarrow S(^3P) + O_2(X^3\Sigma_g^-) \quad \Delta H° = 574 \text{ kJ mol}^{-1} \quad (2)$$

The heats of reactions were calculated from the heats of formation recommended by NASA/JPL.[16] Channel 1 is the only possible path in the present study, because the reported threshold wavelengths of channels 1 and 2 are at 219.2 nm[17] and shorter than 180 nm, respectively.[18] The number density of SO($X^3\Sigma^-$) generated in the photolysis, n, is given by the following equation:[7]

$$n = n_0\phi[1 - \exp(-\rho\sigma)] \quad (3)$$

where n_0 is the concentration of parent molecule (SO_2), ϕ is the quantum yield of photofragment (SO), ρ is the area photon density of the photolysis laser, and σ is the photoabsorption cross section of parent molecule. ρ is estimated to be $\leq 10^{15}$ cm^{-2} from the energy density of the photolysis laser at the entrance window of the reaction cell (≤ 1 mJ cm^{-2}), σ is reported to be 7.9×10^{-18} cm^2 and 6.3×10^{-18} cm^2[7,19] and $\phi \approx 1$.[20] Thus, n is calculated to be $\leq 7 \times 10^{11}$ cm^{-3} at typical pressure (3 mTorr) of SO_2.

The vibrational levels $v' = 0-3$ of SO($B^3\Sigma^-$) were excited via the 0−2, 1−1, 2−2, and 3−2 bands in the $B^3\Sigma^-$-$X^3\Sigma^-$ system with a frequency-doubled dye laser (Lambda Physik LPD3002 with LD489/MeOH and BBO crystal) pumped with a Nd^{3+}:YAG laser (Spectron SL803). The line width (full width at half-maximum, fwhm) of the dye laser is $\Delta\tilde{\nu} = 0.3$ cm^{-1}. Fluorescence from SO($B^3\Sigma^-$) was collected with a quartz lens (f = 80 mm), focused on the entrance slit of a monochromator [JEOL JSG-125S, f = 125 cm, $\Delta\lambda$ (fwhm) = 3 nm], and detected with a photomultiplier tube (PMT) (Hamamatsu R928). The wavelength dependence of the detectivity of the photo detection system was calibrated with a super-quiet Xe lamp (Hamamatsu L2273). The step motor of the monochromator also was controlled with the computer interface (Stanford Research System SR-245) and a typical scanning rate was 8 nm min^{-1}. The number of data points in a dispersed fluorescence spectrum was 4000. All the rotational lines of a single vibrational band are included in the spectral bandwidth of the monochromator (fwhm = 3 nm). The output from the PMT was averaged with a gated integrator (Stanford Research System SR-250) after being amplified [homemade preamp with LF356 (× 10)]. A recorded data point represents averaged signals from 10 laser pulses. The averaged signals were digitized with the computer interface (Stanford Research System SR-245) and stored on a disk of a PC after A/D conversion. Dispersed fluorescence spectra were recorded at different buffer gas pressures (1−200 Torr).

To measure the fluorescence lifetimes of the vibrational levels of the $B^3\Sigma^-$ state, the time profiles of the fluorescence following excitation to a single vibrational level were recorded. The

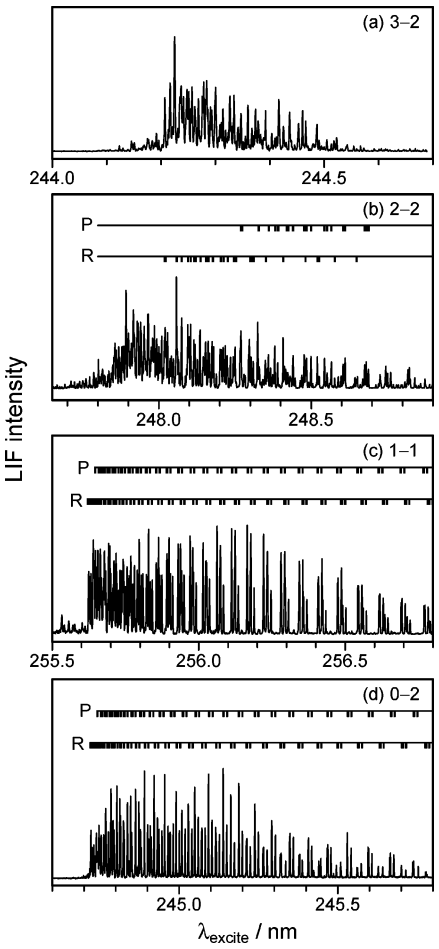

Figure 2. Laser-induced fluorescence excitation spectra of the $B^3\Sigma^-$−$X^3\Sigma^-$ system of SO. The rotational lines of the (a) 3−2 band cannot be assigned because of lack of information on rotational term values. The lines in the (b) 2−2 band are partly assigned after ref 7. All the rotational lines in the spectra of the (c) 1−1 and (d) 0−2 bands are assigned to the P- and R-branches.

TABLE 1: Excited and Observed Vibrational Bands of the SO($B^3\Sigma^-$ − $X^3\Sigma^-$) System

v'	excited band	excited rotational line[a]	λ_{ex}/nm[b]	observed band	λ_{obs}/nm
0	0−2	$P_{11}(17) + P_{33}(17)$	256.16	0−12	350.8
1	1−1	$P_{11}(15) + P_{33}(15)$	245.14	1−14	368.5
2	2−2	$R(20)$[c]	248.30	2−17	401.2
2	2−2	$R(14)$[c]	248.06	2−17	401.2
3	3−2	[d]	244.23	3−19	423.1

[a] The labels of rotational lines are defined to be $\Delta N_{ij}(N'')$ where N is the quantum number of total angular momentum without electronic spin and the subscripts i and j represent spin sublevels of upper and lower states. [b] Wavelengths in the air. [c] Spin sublevels are not assigned. [d] The rotational quantum number is not known.

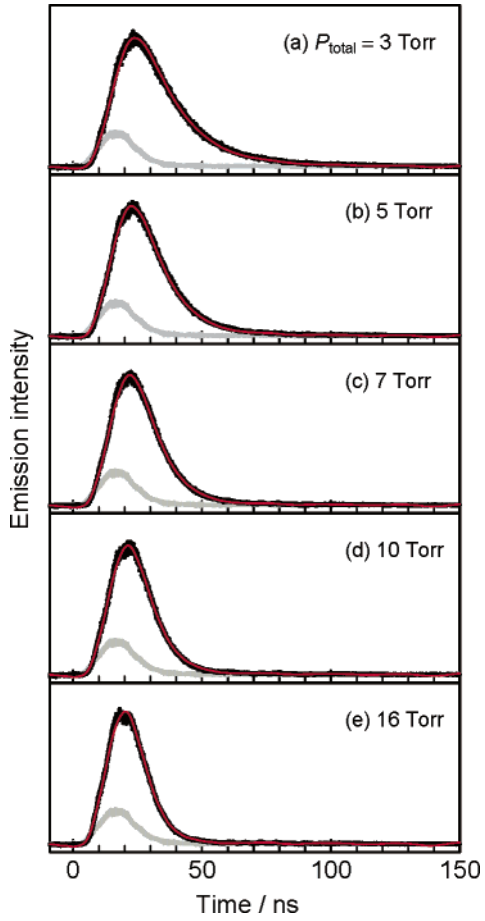

Figure 3. Time-resolved fluorescence from SO($B^3\Sigma^-$, $v' = 3$) excited via the 3−2 bands in the $B^3\Sigma^- - X^3\Sigma^-$ system at various total (Ar) pressures. The partial pressure of SO_2 was 3 mTorr. The large signals shown by the black dots represent fluorescence signal $I(t)$, the small signals (gray dots) are the time profiles of the excitation laser $L(t)$, and the red lines show the convoluted signals calculated by eq 12.

wavelengths of the monochromator were tuned to the 0−12 (350.8 nm), 1−14 (368.5 nm), 2−17 (401.2 nm), 3−19 (423.1 nm) bands, respectively, for monitoring the fluorescence from $v' = 0-3$. These vibrational bands detected with a resolution of 3 nm do not overlap with any other bands of the $B^3\Sigma^- - X^3\Sigma^-$ system, and fluorescence from a single vibrational level can be detected using these bands even if vibrational relaxation populates different vibrational levels of SO($B^3\Sigma^-$). When the fluorescence decay curves were recorded, the output from the PMT was fed into a digital oscilloscope (Tektronix TDS420A, effective time resolution: 20 ps, sampling data points: 15 000) after being amplified [Stanford Research System SR-445 (× 25)] and the signals from 10 000 laser pulses were averaged. The applied voltage to the PMT remained constant during all the measurements of time profiles, because the response time of the PMT depends on the applied voltage. We, therefore, adjusted the time delays between the photolysis and excitation (5 μs−1 ms) and varied the number of molecules excited to the $B^3\Sigma^-$ state to gain appropriate laser-induced fluoresence (LIF) signal intensities. The oscilloscope was triggered with an output from a PIN photodiode (Hamamatsu S1722−02) detecting the light of the YAG laser. When the time profiles of excitation laser pulse were recorded, the wavelength of the monochromator was tuned to that of excitation laser and scattered light in the cell was detected. At least three profiles were recorded and averaged to obtain a sufficient signal-to-noise ratio.

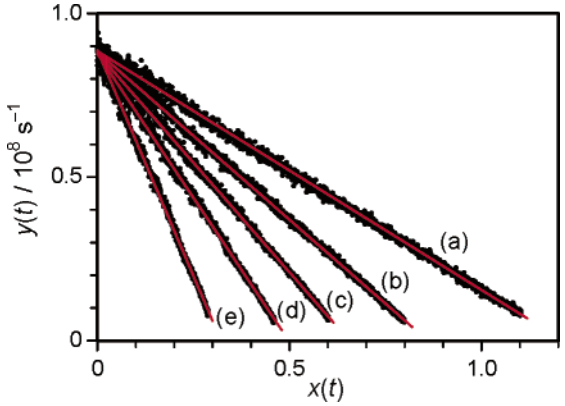

Figure 4. Plots of the integrated-profiles analysis made by the time profiles of the fluorescence from SO($B^3\Sigma^-$, $v' = 3$) shown in Figure 3. Total pressures (Ar) were: (a) 3 Torr, (b) 5 Torr, (c) 7 Torr, (d) 10 Torr, and (e) 16 Torr. The $y(t)$ and $x(t)$ are defined by eq 11 in the text. The red lines show the results of a linear regression analysis and the slopes give the first-order deactivation rates of the excited levels.

The flow rates of all the sample gases were controlled with calibrated mass flow controllers (Tylan FC-260KZ and STEC SEC-400 mark3) and mass flow sensors (STEC SEF-410). The linear flow velocity was 10 cm s^{-1} irrespective of buffer gas pressures. The total pressures of the buffer gases were monitored with a capacitance manometer (Baratron 122A). The total pressure measurement together with the mole fractions as measured by the flow controllers gave the partial pressures of the reagents. The cylinders of sample gases, SO_2 (>99.9%), Ar (>99.9999%), and N_2 (>99.9999%), were delivered by Nihon Sanso, and used without further purification.

Results and Discussion

LIF Excitation Spectra of SO($B^3\Sigma^- - X^3\Sigma^-$). Figure 2, parts a−d, shows the laser-induced fluorescence excitation spectra of the 3−2, 2−2, 1−1, and 0−2 bands in the $B^3\Sigma^- - X^3\Sigma^-$ system of SO. The rotational lines of 0−2 and 1−1 band are assigned to the main branches using reported spectroscopic data.[8,9,21−24] No decisive rotational assignment for $v' = 2$ has been reported and the lines tentatively analyzed by Stuart et al.[7] are shown in Figure 2b. None of the rotational lines of the 3−2 band is assigned because all the rotational levels of the $v' = 3$ are strongly perturbed[25] and no accurate rotational constants or term values of $v' = 3$ have been reported. The vibrational bands for excitation and observation are listed in Table 1.

Radiative Lifetimes and Deactivation Rates of SO($B^3\Sigma^-$). Figure 3 shows the time-resolved fluorescence following excitation to $v' = 3$ at different buffer gas (Ar) pressures. All the profiles are normalized by their maximum intensities. Simple semilogarithmic analysis is not applicable to determine the apparent fluorescence decay rates because the duration of excitation laser is not sufficiently short compared to the decay period of fluorescence. Therefore, deconvolution analysis[26] based on the integrated-profiles method[27,28] has been made to derive fluorescence decay rates.

The possible fates of an excited single vibrational level of SO($B^3\Sigma^-$, v') are represented by the following scheme:

$$SO(X,v) + h\nu \xrightarrow{E(t)} SO(B,v') \quad (4)$$

$$SO(B,v') \xrightarrow{k_r} SO(X,v'') + h\nu' \quad (5)$$

$$SO(B,v') + M \xrightarrow{k_Q} SO(Y) + M \text{ or } S + O + M \quad (6)$$

$$SO(B,v') + M \xrightarrow{k_v} SO(B,v' - \Delta v) + M \quad (v' \geq 1) \quad (7)$$

$E(t)$ is the time-dependent rate of excitation in units of molecule cm^{-3} s^{-1}. k_r is the rate coefficient for radiative decay, k_v and k_Q are the rate coefficients for vibrational relaxation and quenching by collisions with M (M = Ar or N_2). SO(Y) in process 6 represents a nonfluorescent electronic state. The rate equation for the initially prepared vibrational level SO(B,v') is

$$\frac{d[SO(B,v')]}{dt} = E(t) - \{k_r + (k_v + k_Q)[M]\}[SO(B,v')] \quad (8)$$

and it can be transformed into the following equation for deactivation[27,28]

$$I(t) = C\int_0^t L(t')dt' - k\int_0^t I(t')dt' \quad (9)$$

where $I(t)$ is a time-resolved fluorescence intensity, $I(t) = C_1[SO(B,v')]$, $L(t)$ is the intensity profile of the excitation, $L(t) = C_2E(t)$, C is the ratio of the constants C_1/C_2, and k $\{= k_r + (k_v + k_Q)[M]\}$ is an apparent first-order deactivation rate at a given pressure of M. The following linear regression equation is obtained:

$$y(t) = -kx(t) + C \quad (10)$$

where

$$x(t) \equiv \int_0^t I(t')dt' / \int_0^t L(t')dt' \text{ and } y(t) \equiv I(t') / \int_0^t L(t')dt' \quad (11)$$

Thus, a plot of $y(t)$ versus $x(t)$ gives a straight line with a slope k and an intercept C. Typical plots are shown in Figure 4 which is made by the profiles shown in Figure 3.

We also have calculated the convolution integrals[26]

$$I(t) = C\int_0^t L(t') \exp[-k(t - t')]dt' \quad (12)$$

to confirm whether the values of apparent decay rates determined by deconvolution are reliable. Calculated $I(t)$ using eq 12 is shown in Figure 3 and all the observed profiles are well-reproduced. All the deactivation rates of other vibrational levels $v' = 0-2$ also have been obtained in the same manner.

The buffer gas pressure dependence of the first-order fluorescence decay rates is shown in Figure 5. The slopes of the straight line fit from regression analysis give the second-order rate coefficients for deactivation of vibrational levels of SO($B^3\Sigma^-$) by collisions with Ar and the intercepts correspond to the collision-free (radiative) lifetimes. While the radiative lifetimes of the four vibrational levels are nearly identical and independent of the collision partners, deactivation rate coefficients are strongly dependent on the vibrational levels. Because the collisional deactivation of $B^3\Sigma^-$ ($v' = 1-3$) is due to vibrational relaxation and quenching ($k_v + k_Q$), rate coefficients for vibrational relaxation or quenching need to be determined to evaluate the contributions of both processes to deactivation of SO($B^3\Sigma^-$).

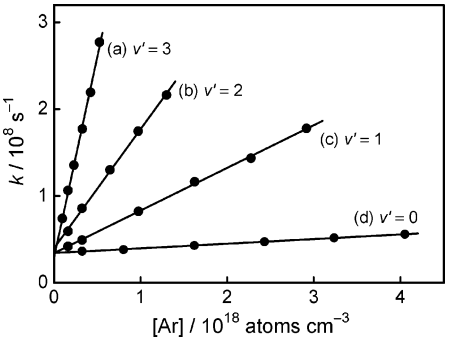

Figure 5. Total pressure dependence of the first-order decay rates of SO($B^3\Sigma^-$, v') by collisions with Ar. The ordinate represents the overall decay rate coefficient defined by $k_r + (k_v + k_Q)$[Ar] in eq 8.

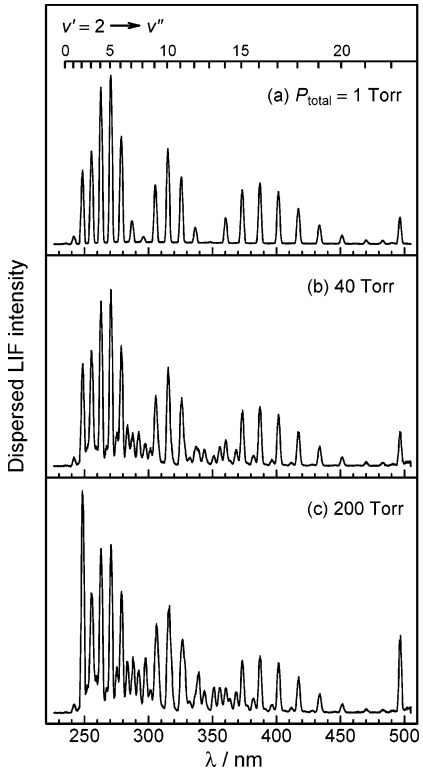

Figure 6. Dispersed fluorescence spectra of the $B^3\Sigma^-$-$X^3\Sigma^-$ system of SO excited to a single vibrational level ($v' = 2$) at different total pressure of a buffer gas (Ar). The partial pressure of SO_2 was 3 mTorr. The assignment shown in part (a) is the transition wavelength of the 2-v'' progression. The new peaks appearing in parts (b) and (c) are the fluorescence from the levels $v' = 0$ and 1 populated by vibrational relaxation by collisions with Ar.

Level-to-Level Vibrational Relaxation of SO($B^3\Sigma^-$). Figures 6 shows typical dispersed fluorescence spectra on excitation to a single vibrational level ($v' = 2$) at different buffer gas (Ar) pressures. The peaks at ≈248 and ≈496 nm are the first- and second-order diffracted lights of the scattered excitation laser. The spectrum shown in Figure 6a was recorded at 1 Torr and all the fluorescence peaks are assigned to 2-v'' bands of the $B^3\Sigma^-$-$X^3\Sigma^-$ system. At high buffer gas pressures, new peaks assignable to the 1-v'' and 0-v'' bands also appear as shown in Figure 6, parts b and c, indicating that vibrational relaxation in the $B^3\Sigma^-$ state occurs by collisions with Ar.

Dispersed fluorescence spectrum on excitation to a level v', $A_{v'}(\lambda)$, consists of fluorescence from v ($\leq v'$), $F_v^{(v')}(\lambda)$, and scattered laser light, $L_{v'}(\lambda)$:

$$A_{v'}(\lambda) = \sum_{v} F_{v}^{(v')}(\lambda) + L_{v'}(\lambda) = \sum_{v} a_{v}^{(v')} f_{v}(\lambda) + b_{v'} l_{v'}(\lambda) \tag{13}$$

where $f_v(\lambda)$ represents the dispersed fluorescence spectrum of a level v recorded at low total pressures (1 Torr) at which vibrational relaxation hardly occurs, $l_{v'}(\lambda)$ is the spectrum of the scattered laser light on excitation to a level v', and $a_v^{(v')}$ and $b_{v'}$ are the weights of the component $f_v(\lambda)$ and $l_{v'}(\lambda)$, respectively. The values of $a_v^{(v')}$ and $b_{v'}$ can be obtained with a least-squares analysis using eq 13.

The kinetic scheme of SO($B^3\Sigma^-$, v) is given by processes 5, 6, and 7. We shall henceforth write the rate coefficients for radiative decay of a level v, k_{rv}; electronic quenching of a level v, k_{Qv}; and vibrational relaxation $v \rightarrow j$, k_{vj}. The rate equation of a vibrational level v following excitation to vibrational level v' is given by

$$\frac{dN_v^{(v')}(t)}{dt} = \sum_{i=v+1}^{v'} k_{iv}[M]N_i^{(v')}(t) - \{k_{rv} + (k_{Qv} + \sum_{j=0}^{v-1} k_{vj})[M]\}N_v^{(v')}(t) \tag{14}$$

where $N_v^{(v')}(t)$ is the number of molecules in a level v at time t after excitation to a level v'. The intensity of fluorescence from the level v at time t, $I_v^{(v')}(t)$, is related to the population in the level v by $I_v^{(v')}(t) = k_{rv}N_v^{(v')}(t)$ and integration of eq 14 from $t = 0$ to ∞ gives

$$\sum_{i=v+1}^{v'} \frac{k_{rv}}{k_{ri}} k_{iv}[M] \int_0^\infty I_i^{(v')}(t)dt = \{k_{rv} + (k_{Qv} + \sum_{j=0}^{v-1} k_{vj})[M]\} \int_0^\infty I_v^{(v')}(t) \tag{15}$$

Since the entire time history of the $B^3\Sigma^-$ state population is collected with the sampling gate, the integrated fluorescence intensities are replaced with the areas of component fluorescence $S_v^{(v')}$. $S_v^{(v')}$is calculated by $\int a_v^{(v')} f_v(\lambda)d\lambda$ and the kinetic analysis of level-to-level vibrational relaxation can be made by the following equations derived by eq 15.[13−15] For the sake of simplicity, the coefficient of the integral on the right side of eq 15 is written by k_v. For single-quantum relaxation ($\Delta v = 1$; $v \rightarrow v - 1$)

$$\frac{S_v^{(v)}}{S_{v-1}^{(v)}} = \frac{k_{rv}}{k_{v,v-1}} \frac{1}{[M]} + \frac{k_{rv}k_{v-1}}{k_{r,v-1}k_{v,v-1}} \tag{16}$$

for double-quantum relaxation ($\Delta v = 2$; $v \rightarrow v - 2$)

$$\frac{S_v^{(v)}}{S_{v-2}^{(v)} - aS_{v-2}^{(v-1)}} = \frac{k_{rv}}{k_{v,v-2}} \frac{1}{[M]} + \frac{k_{rv}k_{v-2}}{k_{r,v-2}k_{v,v-2}} \tag{17}$$

and for triple-quantum relaxation ($\Delta v = 3$; $v \rightarrow v - 3$)

$$\frac{S_v^{(v)}}{S_{v-3}^{(v)} - aS_{v-3}^{(v-1)} - (c - ab)S_{v-3}^{(v-2)}} = \frac{k_{rv}}{k_{v,v-3}} \frac{1}{[M]} + \frac{k_{rv}k_{v-3}}{k_{r,v-3}k_{v,v-3}} \tag{18}$$

where $a \equiv S_1^{(2)}/S_1^{(1)}$, $b \equiv S_2^{(3)}/S_1^{(2)}$, and $c \equiv S_1^{(3)}/S_1^{(1)}$. Typical plots based on eq 17 are shown in Figure 7. The radiative decay rates k_{rv} have already been determined and the level-to-level vibrational relaxation rate coefficients $k_{v,v-1}$, $k_{v,v-2}$, and $k_{v,v-3}$ can be determined from the reciprocals of the slopes of the plots using eqs 16−18. The rate coefficients of level-to-level relaxation determined by the present study are listed in Table 2 along with those in the previous study using He.[14,15]

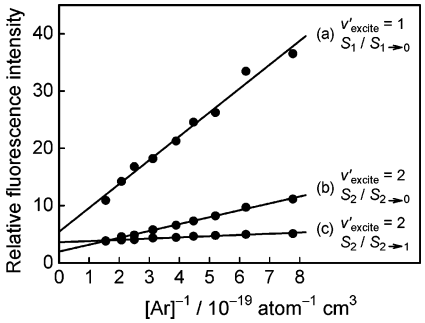

Figure 7. Total pressure dependence of relative fluorescence intensities on excitation to $v' = 1$ and 2. Note that the abscissa is a reciprocal total pressure. v'_{excite} represents the initially prepared vibrational level. The ordinates represent (a) $S_1^{(1)}/S_0^{(1)}$, (b) $S_2^{(2)}/(S_0^{(2)} - aS_0^{(1)})$, and (c) $S_2^{(2)}/S_1^{(2)}$ for the plots a−c, respectively, (see eqs 16 and 17). The slopes of the straight lines fit from regression analysis correspond to (a) k_{r1}/k_{10}, (b) k_{r2}/k_{20}, and (c) k_{r2}/k_{21} for the plots a−c, respectively.

According to the basic theory for vibrational energy transfer of harmonic oscillator,[29] the probabilities of the energy transfer from vibration to translation ($V-T$) increase with vibrational quantum number v. The overall vibrational relaxation rates ($\Sigma_v k_{v'v}$) of a level $v' = 2$ by the three buffer gases (He, Ar, and N_2) are larger than those of $v' = 1$ by more than an order of magnitude. The efficiency in overall relaxation of $v' = 3$ on the other hand is comparable to those of $v' = 2$. The anomalous relation between overall relaxation rates, $\Sigma_v k_{1v} << \Sigma_v k_{2v} \approx \Sigma_v k_{3v}$, is due partly to the effect of vibrational relaxation followed by quenching. The highest fluorescent rotational level $N' = 10$ of $v' = 3$ is energetically close ($\approx$60 cm^{-1}) to the lowest nonfluorescent level $N' = 38$ of $v' = 2$,[8] and relaxation from $v' = 3$ to the nonfluorescent levels of $v' = 2$ is observed as quenching instead of relaxation. This effect sets the k_{32} values estimated in the present study to a lower limit. This, however, is by no means certain because such a large jump in rotational quantum number might be inefficient.

The efficiency of relaxation with $\Delta v \geq 2$ is usually very small because the selection rule for vibrational relaxation of a harmonic oscillator is $\Delta v = 1$.[29] In the present study, the extraordinarily high contribution of multiquantum relaxation ($\Delta v = 2$ and 3) to overall relaxation has been measured despite small anharmonicity $\omega_e x_e(B^3\Sigma^-) = 2.6$ cm^{-1};[8] $f_{v'v} = k_{v'v}/(\Sigma_v k_{v'v})$ are $f_{20} = 0.10$, 0.15, and 0.11, $f_{31} = 0.57$, 0.72, and 0.47, and $f_{30} = 0.08$, 0.11, and 0.12 for He, Ar, and N_2, respectively. The cause of the high efficiency of multiquantum relaxation might be attributed to the strong coupling between the vibrational levels of $B^3\Sigma^-$ and (an)other unknown electric state(s) (designated Z in this paper). The interactions through the coupled state Z enable the multiquantum relaxation: $B(v' \leq 3) \rightarrow Z(v) \rightarrow B(v' - \Delta v)$ with $\Delta v \neq 1$. In fact, Clerbaux and Colin[8] and Liu et al.[25] have found many perturbed rotational levels in $v' = 0-3$ of the $B^3\Sigma^-$ state. The $C^3\Pi$ and $d^1\Pi$ states are ruled out of the candidates for the coupled states, not only because the levels of $v' = 0$ of the $C^3\Pi$ and $d^1\Pi$ states are located at higher than $v' = 4$ and 3 of the $B^3\Sigma^-$ state, respectively, and neither of $C^3\Pi$ and $d^1\Pi$ interacts with the fluorescent rotational levels of $v' \leq 3$ in the $B^3\Sigma^-$ state but also because the vibrational levels of the $C^3\Pi$ and $d^1\Pi$ states are nonfluorescent due to predissociation.[12] Archer et al.[12] reported that there were unassigned

TABLE 2: Rate Coefficients for Level-to-Level Vibrational Relaxation of SO($B^3\Sigma^-$, $v' = 1-3$)[a]

		k_{if}[d]		
v_i'[b]	v_f'[c]	He[e]	Ar[f]	N_2[f]
1	0	$(7.7 \pm 1.0) \times 10^{-13}$	$(7.7 \pm 2.0) \times 10^{-13}$	$(6.6 \pm 1.0) \times 10^{-13}$
2	0	$(1.4 \pm 0.6) \times 10^{-12}$	$(3.4 \pm 0.5) \times 10^{-12}$	$(5.8 \pm 0.8) \times 10^{-12}$
	1	$(1.1 \pm 0.4) \times 10^{-11}$	$(1.9 \pm 0.5) \times 10^{-11}$	$(4.7 \pm 0.5) \times 10^{-11}$
3	0	$(9.8 \pm 4.0) \times 10^{-13}$	$(2.6 \pm 0.5) \times 10^{-12}$	$(3.6 \pm 1.0) \times 10^{-12}$
	1	$(7.1 \pm 2.3) \times 10^{-12}$	$(1.8 \pm 0.2) \times 10^{-11}$	$(1.4 \pm 0.4) \times 10^{-11}$
	2	$(4.3 \pm 1.2) \times 10^{-12} <$[g]	$(4.2 \pm 1.0) \times 10^{-12} <$[g]	$(1.2 \pm 0.6) \times 10^{-11} <$[g]

[a] The quoted errors are 2σ. [b]Initially prepared vibrational level. [c]Vibrational level generated from v_i by relaxation. [d]In units of cm^3 $molecule^{-1}$ s^{-1}. [e]Refs 14 and 15. [f]This work. [g]A lower limit for k_{32}.

TABLE 3: Rate Coefficients for Quenching of SO($B^3\Sigma^-$, $v' = 0-3$)[a]

	$k_{Qv'}$[b]		
v'	He[c]	Ar[d]	N_2[d]
0	$(6.3 \pm 0.3) \times 10^{-12}$	$(5.4 \pm 0.3) \times 10^{-12}$	$(9.0 \pm 0.5) \times 10^{-12}$
1	$(3.8 \pm 0.3) \times 10^{-11}$	$(4.8 \pm 0.3) \times 10^{-11}$	$(7.5 \pm 0.4) \times 10^{-11}$
2	$(1.2 \pm 0.2) \times 10^{-10}$	$(1.2 \pm 0.2) \times 10^{-10}$	$(8.7 \pm 2.0) \times 10^{-11}$
3	$(2.8 \pm 0.5) \times 10^{-10}$	$(4.4 \pm 0.6) \times 10^{-10}$	$(3.0 \pm 0.5) \times 10^{-10}$

[a] The quoted errors are 2σ. [b]In units of cm^3 $molecule^{-1}$ s^{-1}. [c]Refs 13 and 15. [d]This work.

four bands with well-resolved rotational structure at ≈42 660, ≈43 065, ≈43 155, and ≈43 270 cm^{-1}. The energies of these bands are nearly identical to those of the vibrational levels $v' = 0-2$ of the $B^3\Sigma^-$ state, suggesting that there are unknown electronic states perturbing the levels $v' \leq 3$ of the $B^3\Sigma^-$ state.

The small rate coefficients even by N_2 might be due to the large vibrational energy mismatches between SO($B^3\Sigma^-$, v') and N_2: the vibrational quantum energies between the adjacent levels of SO($B^3\Sigma^-$, $v' = 1-3$) are 607−613 cm^{-1} and the fundamental vibrational energy of N_2 is 2330 cm^{-1}.[30] Therefore, $V-T$ rather than $V-V$ process might govern the energy transfer between SO($B^3\Sigma^-$) and N_2 as well as He and Ar. The contribution of vibrational relaxation in deactivation is small (less than 15%) for all the levels and collision partners. Quenching is a main channel in deactivation and the mechanism is discussed in the following section.

Quenching of SO($B^3\Sigma^-$, $v' = 0-3$). The quenching rate coefficients of SO($B^3\Sigma^-$, v') by collisions with Ar and N_2 determined in the present study are listed in Table 3 along with the values obtained by He.[13-15] The higher vibrational levels are more efficiently quenched by all collision partners. Stuart et al.[7] have measured the deactivation rate coefficient of SO($B^3\Sigma^-$, $v' = 2$) by He to be $(1.3 \pm 0.3) \times 10^{-10}$ cm^3 $molecule^{-1}$ s^{-1}, which is in perfect agreement with ours, although they did not estimate the contribution of vibrational relaxation. They have also measured the saturation fluence of the optically pumped SO(B−X) laser, giving the effective rotational mixing time of $v' = 2$ by He to be 0.4 ns at 100 Torr and 1.3 ns at 30 Torr. The effective rate coefficient for rotational relaxation ≈ 8×10^{-10} cm^3 $molecule^{-1}$ s^{-1}, therefore, is almost gas kinetic and faster than quenching. Unfortunately, there has been no report on rotational relaxation by Ar or N_2. It can be assumed that the efficiency of rotational relaxation by Ar and N_2 is nearly identical with that by He because of the small effect of mass on rotational relaxation.[29]

It is not likely that the efficiency of collisional deactivation to the $X^3\Sigma^-$ state shows the strong dependence on the vibrational levels of the $B^3\Sigma^-$ state. Alternately, the quenching might proceed via a collision-induced transition from the $B^3\Sigma^-$ state to nearby nonfluorescent or dissociating (repulsive) states. The onset of missing rotational levels N^* in emission spectra of the $B^3\Sigma^-$ state is low at high vibrational levels: $N^* = 66$ ($v' = 0$), 54 ($v' = 1$), 38 ($v' = 2$), and 11 ($v' = 3$)[8] and, consequently, quenching efficiency is high at the vibrational levels with small N^*. The fast rotational relaxation plays a role as activation process transferring the initially prepared rotational level to N^*; therefore, the quenching rate coefficient k_Q can be represented by the Arrhenius type formula: $k_Q = A \exp(-E_a/RT)$, in which E_a is an effective activation energy, R is a gas constant, and T is a temperature. According to the Tolman's interpretation[31] of activation energy, E_a is $\langle E_{\text{reactive reactant}} \rangle - \langle E_{\text{all reactant}} \rangle$, where $\langle\ \rangle$ denotes an average over thermal distributions. In the present system, $\langle E_{\text{reactive reactant}} \rangle$ is approximately the energy of the lowest nonfluorescent rotational level E^* and $\langle E_{\text{all reactant}} \rangle \approx RT$, giving $k_Q = A \exp[-(E^* - RT)/RT] = A' \exp(-E^*/RT)$. Logarithmic k_Q is

$$\ln k_Q = -\frac{E^*}{RT} + \ln A' \qquad (19)$$

indicating that the plot of $\ln k_Q$ vs E^* shows a straight line with a slope $-(RT)^{-1}$, where T is an effective rotational temperature of SO. E^* is approximated by a rigid rotor, $E^* = B_{v'}N^*(N^* + 1)$, because the effect of centrifugal distortion of the $B^3\Sigma^-$ state is negligibly small ($D_v \approx 1 \times 10^{-6}$ cm^{-1}): $D_v[N'(N'+1)]^2/[B_{v'}N'(N'+1)] < 1 \times 10^{-2}$ over $N' \leq N^*$. Figure 8 shows the correlation between the logarithm of the quenching rate coefficients and the energies of the lowest nonfluorescent rotational levels. The regression lines of the plots give the transient rotational temperatures of SO($B^3\Sigma^-$): 820 ± 40 K (He), 720 ± 50 K (Ar), and 950 ± 110 K (N_2). The nearly identical rotational temperatures for the three collision partners suggest that the quenching of the $B^3\Sigma^-$ state proceeds via the rotational relaxation followed by a transfer to nonfluorescent states.

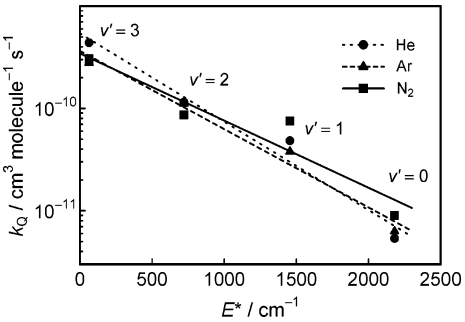

Figure 8. Plots of the quenching rate coefficients vs the rotational energies of the lowest nonfluorescent levels. E^* is given by $B_{v'}N^*(N^* + 1)$, where N^* is the quantum number of the lowest nonfluorescent rotational level.

Ornellas and Borin[10] proposed that the $C^3\Pi$ state is the candidate for governing the quenching of the $B^3\Sigma^-$ state because the rovibrational energies of the first missing levels N^* of $B^3\Sigma^-$ ($v' = 0-3$) correspond to that at the curve crossing of the $B^3\Sigma^-$

and $C^3\Pi$ states. It, however, should be noted that Kronig's selection rules for perturbation[32] requires that both perturbing and perturbed levels have the identical rotational quantum number: $\Delta N = 0$ for the Hund's case (b). The lowest vibrational level of the $C^3\Pi$ state is located higher than $v' = 4$ of the $B^3\Sigma^-$ state and the rotational constant[8] $B_e(C^3\Pi) = 0.578\ cm^{-1}$ is larger than that of the $B^3\Sigma^-$ state ($0.5016\ cm^{-1}$),[12] and as a consequence, none of the rovibrational energies with N' in $v' = 0-3$ of the $B^3\Sigma^-$ state coincides with those with the same N' of the $C^3\Pi$ state. Therefore, the $C^3\Pi$ state hardly relates to the quenching of the levels $v' = 0-3$ of the $B^3\Sigma^-$ state. The $d^1\Pi$ state also is ruled out by the similar reasons: $v' = 0$ of the $d^1\Pi$ state is located higher than $v' = 3$ of the $B^3\Sigma^-$ state and the rotational constant $B_e(d^1\Pi) = 0.562\ cm^{-1}$ is larger than that of $B^3\Sigma^-$.[12] Liu et al.[25] have recently reported that any state of SO correlating with $S(^3P) + O(^3P)$ can interact with the $B^3\Sigma^-$ state and that the $v' = 1$ is perturbed by the $A^3\Pi$ ($v = 10$) and $A'^3\Sigma^+$ states and the $v' = 2$ by the $A'^3\Delta$ and/or $a^1\Delta$ states. The level $v' = 3$ also undergoes significant perturbations although the origin is not identified. Another candidate is the $^5\Pi$ state; however, this state has been found only by the ab initio calculation.[12] Evaluation of the off-diagonal spin−orbit matrix elements $\langle B^3\Sigma^-|H^{SO}|^5\Pi\rangle$ are needed to judge whether the quenching of the $B^3\Sigma^-$ state proceeds via the $^5\Pi$ state.

Summary

The kinetic measurements of the rate coefficients for photochemical processes of $SO(B^3\Sigma^-, v' = 0-3)$ in Ar and N_2 buffer gases have been carried out. The rates of deactivation have been determined from time-resolved fluorescence intensities and the level-to-level vibrational relaxation rates have also obtained by the buffer gas pressure dependence of dispersed fluorescence spectra. Deconvolution using the integrated-profiles method made it possible to determine the fluorescent lifetimes shorter than the temporal width of the excitation laser. Vibrational relaxation k_v is less efficient than quenching k_Q on all the vibrational levels ($k_v/k_Q < 6$). Multiquantum vibrational relaxation ($\Delta v \neq 1$) was observed and its large contribution suggests the presence of unknown perturbing electronic states. The higher vibrational levels undergo more efficient quenching, and the highest fluorescent vibrational level $v' = 3$ is quenched at almost gas kinetic rates irrespective of the collision partners. Quenching proceeds via rotational relaxation followed by a radiationless transition to nearby electronic states.

Acknowledgment. This work was supported by a Grant-in-Aid for Exploratory Research (Contract No. 15655005) and a Grant-in-Aid for Scientific Research (B) (Contract No. 18350011) of the Japanese Ministry of Education, Culture, Sports, Science, and Technology. Support also was provided by Matsuo Foundation.

References and Notes

(1) Clyne, M. A. A.; McDermid, I. S. *J. Chem. Soc., Faraday Trans. 2* **1979**, *75*, 905.
(2) Clyne, M. A. A.; Liddy, J. P. *J. Chem. Soc., Faraday Trans. 2* **1982**, *78*, 1127.
(3) Cao, D. Z.; Setser, D. W. *Chem. Phys. Lett.* **1985**, *116*, 363.
(4) Cao, D. Z.; Setser, D. W. *J. Phys. Chem.* **1988**, *92*, 1169.
(5) Lo, G.; Beaman, R.; Setser, D. W. *Chem. Phys. Lett.* **1988**, *149*, 384.
(6) Miller, H. C.; Yamasaki, K.; Smedley, J. E.; Leone, S. R. *Chem. Phys. Lett.* **1991**, *181*, 250.
(7) Stuart, B. C.; Cameron, S. M.; Powell, H. T. *J. Phys. Chem.* **1994**, *98*, 11499.
(8) Clerbaux, C.; Colin, R. *J. Mol. Spectrosc.* **1994**, *165*, 334.
(9) Martin, E. V. *Phys. Rev.* **1932**, *41*, 167.
(10) Ornellas, F. R.; Borin, A. C. *Mol. Phys.* **1998**, *94*, 139.
(11) Borin, A. C.; Ornellas, F. R. *Chem. Phys.* **1999**, *247*, 351.
(12) Archer, C. P.; Elks, J. M. F.; Western, C. M. *J. Chem. Phys.* **2000**, *112*, 6293.
(13) Yamasaki, K.; Taketani, F.; Tomita, S.; Sugiura, K.; Tokue, I. *J. Phys. Chem. A.* **2003**, *107*, 2442.
(14) Yamasaki, K.; Taketani, F.; Takasago, Y.; Sugiura, K.; Tokue, I. *J. Phys. Chem. A.* **2003**, *107*, 4796.
(15) Yamasaki, K.; Tomita, S.; Takayuki, H.; Taketani, F.; Tokue, I. *Chem. Phys. Lett.* **2005**, *413*, 231.
(16) Sander, S. P.; Friedl, R. R.; Golden, D. M.; Kurylo, M. J.; Huie, R. E.; Orkin, V. L.; Moortgat, G. K.; Ravishankara, A. R.; Kolb, C. E.; Molina, M. J.; F.-Pitts, B. J. *Chemical Kinetics and Photochemical Data for Use in Atmospheric Studies, Evaluation No. 14*; Jet Propulsion Laboratory, California Institute of Technology, Pasadena, CA, 2003.
(17) Katagiri, H.; Sako, T.; Hishikawa, A.; Yazaki, T.; Onda, K.; Yamanouchi, K.; Yoshino, K. *J. Mol. Struct.* **1997**, *413−414*, 589.
(18) Okabe, H. *J. Am. Chem. Soc.* **1971**, *93*, 7095.
(19) Okabe, H. *Photochemistry of Small Molecules*; Wiley: New York, 1978.
(20) Hui, M.-H.; Rice, S. A. *Chem. Phys. Lett.* **1972**, *17*, 474.
(21) Norrish, R. G. W.; Oldershaw, G. A. *Proc. R. Soc. London, Ser. A.* **1959**, *249*, 498.
(22) Powell, F. X.; Lide, D. R., Jr. *J. Chem. Phys.* **1964**, *41*, 1413.
(23) Colin, R. *Can. J. Phys.* **1969**, *47*, 979.
(24) Kanamori, H.; Butler, J. E.; Kawaguchi, K.; Yamada, C.; Hirota, E. *J. Mol. Spectrosc.* **1985**, *113*, 262.
(25) Liu, C.-P.; Elliott, N. L.; Western, C. M.; Lee, Y.-P.; Colin, R. *J. Mol. Spectrosc.* **2006**, *238*, 213.
(26) Demas, J. N. *Excited State Lifetime Measurements*; Academic Press: New York, 1983.
(27) Yamasaki, K.; Watanabe, A. *Bull. Chem. Soc. Jpn.* **1997**, *70*, 89.
(28) Yamasaki, K.; Watanabe, A.; Kakuda, T.; Tokue, I. *Int. J. Chem. Kinet.* **1998**, *30*, 47.
(29) Yardley, J. T. *Intramolecular Energy Transfer*; Academic Press: New York, 1980.
(30) Herzberg, G. *Molecular Spectra and Molecular Structure, IV. Constants of Diatomic Molecules*; Van Nostrand Reinhold: New York, 1979.
(31) Levine, R. D.; Bernstein, R. B. *Molecular Reaction Dynamics and Chemical Reactivity*; Oxford: New York, 1987; Chapter 6.
(32) Herzberg, G. *Molecular Spectra and Molecular Structure, I. Spectra of Diatomic Molecules*; Van Nostrand Reinhold: New York, 1950.